

Structure–Behavior–Property Relationship Study of Surfactants as Foam Stabilizers Explored by Experimental and Molecular Simulation Approaches

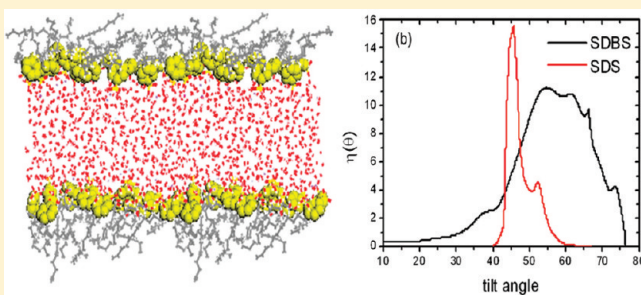
Xiaoying Hu,[†] Ying Li,^{†,*} Xiujuan He,[†] Chunxiu Li,[†] Zhengquan Li,[‡] Xulong Cao,[‡] Xia Xin,[†] and P. Somasundaran[§]

[†]Key Laboratory for Colloid and Interface Chemistry of State Education Ministry, Shandong University, ShanDa South Road, Jinan, Shandong 250100, P. R. China

[‡]Geological Scientific Research Institute, Shengli Oilfield, Dongying 257015, P. R. China

[§]Langmuir Center for Colloids and Interfaces, Columbia University, New York, New York 10027, United States

ABSTRACT: A multiscale stability study of foams stabilized by sodium dodecyl sulfate (SDS), sodium dodecylbenzene sulfonate (SDBS), and sodium polyoxyethylene alkylether sulfate (AES) was conducted, to investigate the relationship of surfactant molecular behavior and interfacial monolayer configuration of foam film to the foam film properties. Molecular dynamic (MD) simulations using a full-atom model was utilized to explore the microscopic features of the air/liquid interface layer. Several parameters such as the distribution of surfactant head groups and the order degree of surfactant hydrophobic tails were used to describe the molecular adsorption behavior. The effect of molecular structure on the nature of the foam film and the impact on the dynamic stability of wet foam is discussed. In the experimental evaluation, the SDBS foam films manifest strong stiffness and low viscoelasticity as shown by the interfacial shear rheology determination as well as texture analyzer (TA) measurement results, which agree very well with the array behavior of SDBS molecules at the air/water interface as described by the simulation results and is identified to be the reason for the poor dynamic stability. Comparing the molecular structure of SDS, SDBS, and AES, the special contributions of the linking groups such as the O atom, the phenyl group, and the EO (oxyethyl) chain to the interfacial array behavior of surfactants were characterized. It is concluded that microhardness of the foam film enhanced by rigid linking groups favors static foam stability but decreases the dynamic foam stability, while viscoelasticity of the foam film enhanced by soft linking groups increases the dynamic foam stability.



1. INTRODUCTION

Foam is a type of gas–liquid dispersed system of great importance, widely used in daily life and for industrial purposes, such as extinguishing fires, mineral floatation, enhanced oil recovery, and detergents.^{1–3} As a thermodynamically unstable system, its stability is always treated as one of the most important features and is commonly characterized by parameters such as the height or volume of the foam column^{4–6} and the volume of the solution draining out of the foam in dependence on time.⁷ Foam used in the above applications is freshly produced with high water content, sometimes by a flowing procedure which is inevitably disturbed, so evaluation of the dynamic foam stability under disturbance is very important, while relative experimental determination methods and theoretical discussions are very scarce.

The size and time scale of foam systems in the practical process could be in meters or years, but the character of foam films, the length scale of which should be in nanometers to micrometers, determines the foam properties, and the array behavior of surfactant molecules on the foam films influences capacities of foam fundamentally. As it is well-known, the disjoining pressure

of foam films is supposed to be the decisive element influencing stability for metastable foams under quasistatic conditions,^{8,9} and many researchers have used electrical or steric repulsions and structural forces to explain the static foam stability.^{10,11} For the wet foam in flowing or under disturbance forms, foam films are deformed frequently. The Gibbs–Marongoni effect^{12,13} is widely used to explain the dynamic foam stability, and the viscoelasticity of foam film is thought to be an important factor that affects the drainage process and the film stability under dynamic disturbances.¹⁴ Evaluation of the foam film feature under disturbance and the description of the molecular interfacial behavior of foam films are both vital for a better understanding of the mechanism of foam dynamic stability to clarify the relationship between the surfactant structure and its foam performance.

A variety of modern experimental techniques, including interfacial rheology,^{15,16} resonance Raman scattering,¹⁷ X-ray reflection,¹⁸

Received: June 20, 2011

Revised: November 28, 2011

Published: December 02, 2011

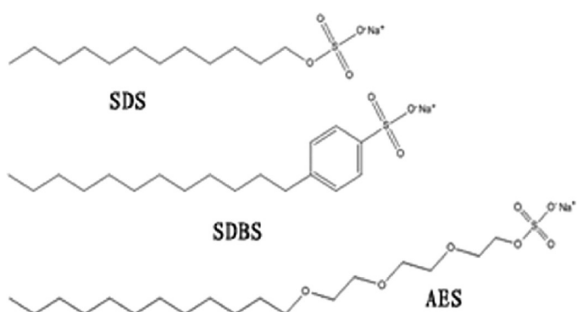


Figure 1. The structures of surfactants used in this study.

and second harmonic generation,¹⁹ have been used to investigate the interfacial composition of various foam systems, but the specific structure of films and the behavior of amphiphilic molecules at foam films could only be understood by inference. In recent years, computer simulations have become an important tool for studying such complex interfacial systems^{20–25} because of the substantial increase in computational power, which makes it possible to extract more detailed information on a molecular level to understand the effect of surfactant behavior and the film structure on the apparent foam properties.

In this paper, the relationship of monolayer configuration in wet foam films to the dynamic stability is analyzed through a combination of molecular simulation and experimental results. Surfactants SDS, SDBS, and AES (see Figure 1), which have similar hydrophobic tails but different hydrophilic heads, were used as foam stabilizers. The relationship between surfactant behavior and foam stability was elucidated by gradual study of the following three stages: (I) evaluation of apparent foam stabilities; (II) evaluation of the foam film feature; (III) microstructure description of foam films by molecular simulation. Not only static stability, but also dynamic stability, of foams was investigated in stage I. In the second stage, a texture analyzer, often used to measure kernel hardness in crop and food engineering research,^{26–28} provided the objective quantitative measurement of the compressing and dragging force on foam films in the vertical direction, which reflects the stiffness and viscoelasticity of the foam film, and the interfacial rheology measurement conducted with a AR2000 rheometer provided the viscoelasticity data of foam films via rotary shearing.²⁹ Eventually, the details of the array of molecules in foam films were investigated by molecular dynamics (MD) simulations using a full-atom model. The special behavior conducted by the different linking groups of the three surfactants was characterized, and the effect of molecule behavior on foam film character and foam stability was discussed.

2. EXPERIMENTAL SECTION

2.1. Materials. Sodium dodecylbenzene sulfonate (SDBS) and sodium polyoxyethylene alkylether sulfate (AES) were of the same origin as documented previously.³⁰ Sodium dodecyl sulfate (SDS) was obtained from Sigma-Aldrich and used without further purification. Freshly distilled water (twice distilled) was used in all solution preparations.

2.2. Measurement. *2.2.1. Static and Dynamic Foam Stability Measurements.* Static stability of foam film with the temperature being no higher than 80 °C is effectively shown by the foam decay curve, which describes the changes of volume of the foam column with time. Measurements were carried out immediately after the

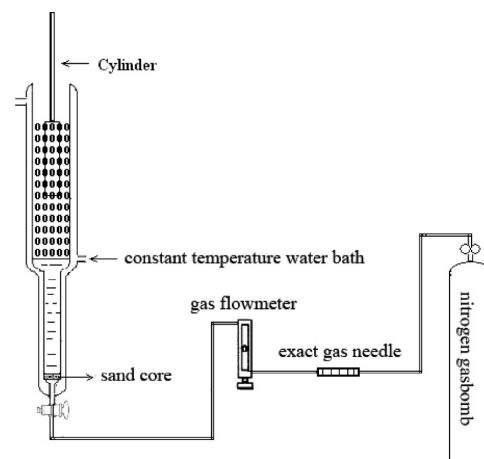


Figure 2. The schematic diagram of the device used in the dynamic stability measurement. The constant temperature water bath ensures that the stability of the foam systems can be determined at the same temperature.

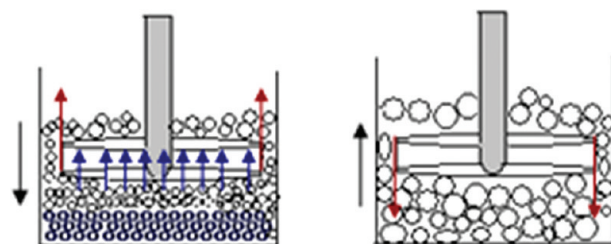


Figure 3. Force analysis of the extrusion disk during the measuring process. Falling procedure (left): bottom resistance (elastic force) and side viscoelastic force; pulling procedure (right): side viscoelastic force (weight of the few foams on top of the disk can be negligible).

certain foam column was generated by nitrogen flow (75 mL/min) method³¹ under conditions without any external disturbance. In this experiment, all the solutions were evaluated by the same device with an equal gas volume injection, and the half-life time (t_{half}) of the foam column was recorded. As for the determination of the dynamic stability, a Brookfield DV-I viscometer with a cylinder rotor (No. 2, 30 r/min) was used to measure the overall foam viscosity after the foam column was generated. The schematic diagram of the device is shown in Figure 2.

2.2.2. Texture Analyzer (TA). The microhardness and the viscoelastic feature of foam films were determined with a texture analyzer (TA-XT2, SMS Stable-Micro-System, UK). Initially, a known volume of wet foam was placed inside a cylindrical cell (100 mm i.d.) that was placed on the sample platform. Then, the extrusion disk was controlled by the computer workstation to depress the sample with a constant speed (0.5 mm/s). When the extrusion disk came through the target distance, it went backward to its departure place. Over the whole process, pressure on the bottom and sides of the disk was recorded with the time or distance varying. The peak compressing force and the viscoelastic force apparently indicated the compressing and dragging peak pressure in the falling and pulling procedure, which qualitatively corresponded to the stiffness and the viscoelasticity of the foam film (see Figure 3).

2.2.3. Interfacial Shear Rheology (RH). All the rheological measurements were performed at 25 °C using a controlled stress

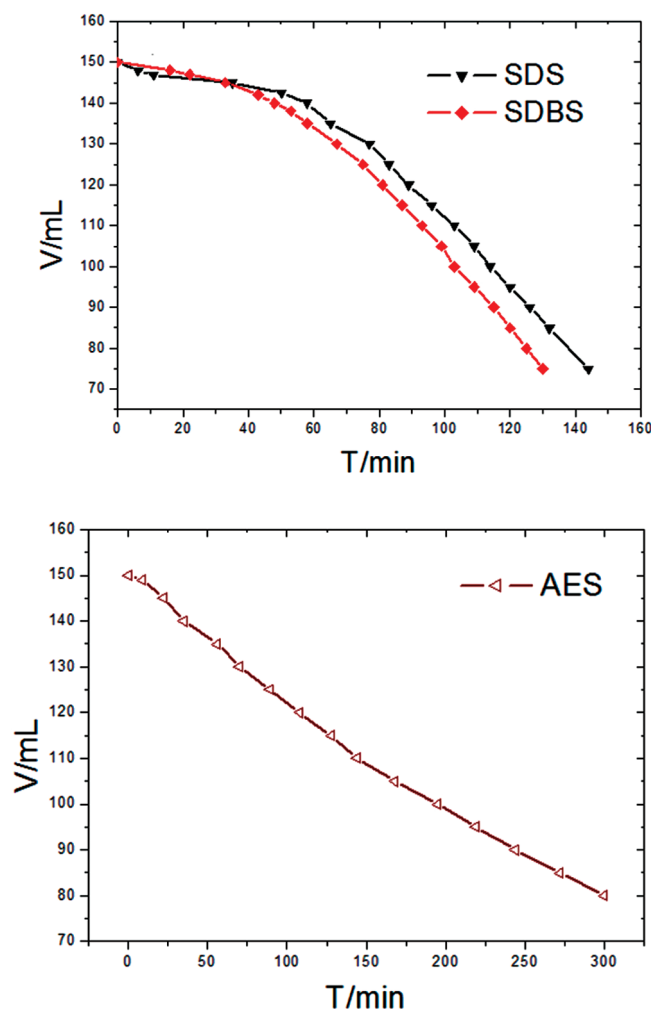


Figure 4. The decay curves of foams formed from different surfactant solutions. \blacklozenge , 0.1%wt SDBS; \blacktriangledown , 0.1%wt SDS; \triangle , 0.075%wt AES, $T = 298\text{ K}$.

rheometer AR2000 (TA Instruments) assembled with an acrylic parallel plate (60 mm i.d.). After 1 mL of wet foam was placed on the sample platform, the parallel plate was moved down until the distance between the sample platform and parallel plate was 0.1 mm. The shearing frequency was kept at 6.284 r/s. Elastic modulus (storage modulus) G' characterizes the solid-like property, and the larger the stiffness of foam film the worse the deformability of foam films. The viscous modulus G'' , also defined as loss modulus, represents the dissipated portion. If the rheological phase angle³² $\delta = \tan(G'/G'')$ is closer to 0° , this means the elasticity of the foam films is better, while a δ value closer to 90° means better film viscosity.

2.3. Molecular Simulation. A reasonable double-layer film model was prepared for the simulation of the wet foam films.^{33,34} To construct the foam film model of each surfactant, 16 surfactant molecules were disposed to form a surfactant monolayer at first, with space suitable for hexagonal close packing in a simulation box imposed to periodic boundary conditions in all three spatial directions similar to those shown previously.^{20,35} The size of the simulation box refers to the maximum adsorption area data of surfactants used in previous simulation and experimental results.^{20,36} Then, a 35 Å thick slab of the water phase (the number of water molecules is 800) using the flexible SPC model with the same cell parameters as those of the surfactants cell was

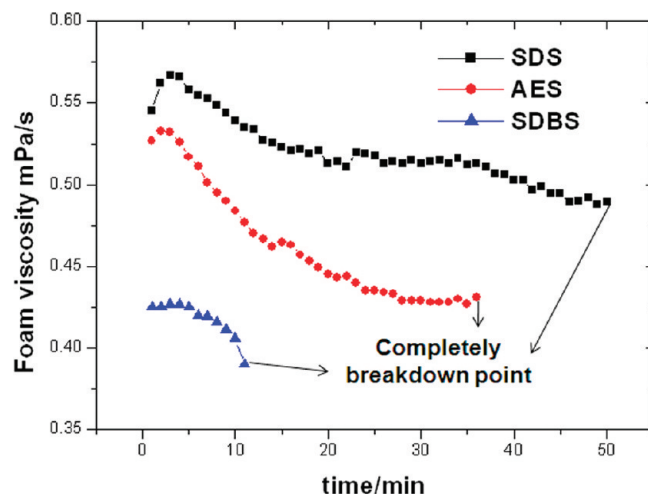


Figure 5. Variation of dynamic overall viscosity of foams formed from different surfactant solutions disturbance conditions under rotation. ■, 0.1%wt SDS; ●, 0.1%wt SDBS; ▲, 0.1%wt AES.

set, and two surfactant monolayers were placed on opposite sides of the water phase with hydrophilic head groups of surfactants inserted.³⁴ As the air phase in the simulation, a vacuum in the direction normal to the bilayer plane was set for the alkyl tail of surfactant extending.³⁵ In the initial configuration, a more than 20 Å thickness of water slab was chosen, the density being close to real water, which ensured that the foam film held up abundant liquid and that the two monolayers of surfactant did not just interact with each other. Therefore, these simulation results can be used to analyze the effects of molecular behavior on the properties of wet foam film.

The charges and potentials of surfactant molecules are assigned to the alkyl tail and the hydrophilic polar head of the surfactant based on the parameters given by the PCFF force field.^{37–39} The total energy of the wet foam film system composed of the contribution of valence is written as:

$$U = U_{\text{bonds}} + U_{\text{angles}} + U_{\text{dihedrals}} + U_{\text{cross}} + U_{\text{VDW}} + U_{\text{elec}}$$

After the full explicit atom model was constructed, molecular dynamic simulation was conducted to explore the interfacial behavior of the surfactants on foam films.

All the systems were equilibrated using MD, which was carried out in the NVT ensemble with a time step of 0.001 ps. The temperature was controlled using a Hoover-Nose thermostat⁴⁰ with a relaxation time of 0.2 ps. The simulations were performed at $T = 298\text{ K}$, being the same as experimental conditions. For the long-range electrostatic potential statistics, the Ewald summation method was used.⁴¹ After a 200 ps MD equilibration period, at least a 1 ns³⁵ MD production was run to obtain the dynamic information using the trajectory of molecules in the simulation box and the properties of the foam film were evaluated. All the simulations were performed in the software Material studio 4.3 by Accelrys.

3. RESULTS AND DISCUSSION

3.1. Experimental Evaluation of Foam Stability. According to Figure 4, the t_{half} of foams formed by anionic surfactants SDS and SDBS are all longer than 80 min under the same formation conditions at 298 K. The foam decay curves both show a slight

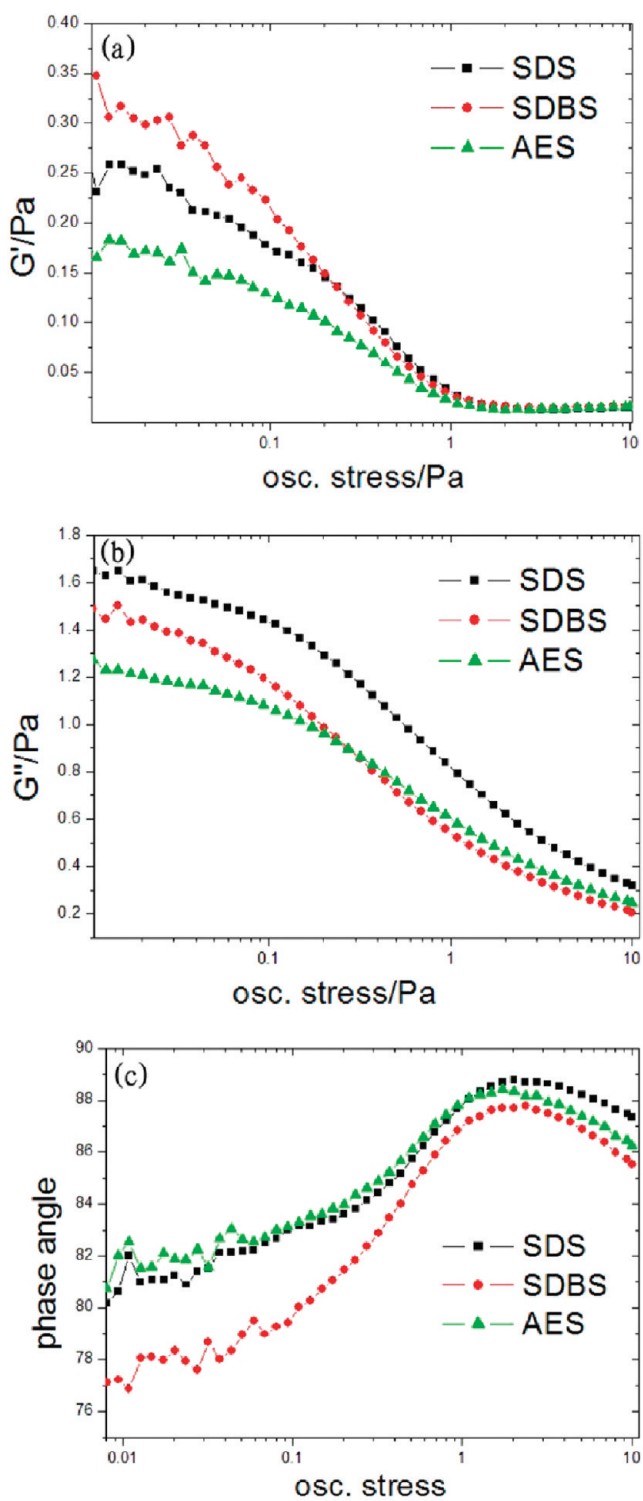


Figure 6. The variation of (a) the elastic modulus G' , (b) the viscous modulus G'' , and (c) the phase angle of the foam films stabilized by different types of surfactants as a function of oscillating stress determined with a AR2000 rheometer. ■, 0.1%wt SDS; ●, 0.1%wt SDBS; ▲, 0.1%wt AES.

decrease at the beginning, which indicates that the foam experienced a pure drainage process in this period.⁴¹ Subsequently, a marked decline of the foam volume was caused by a collapsing procedure. In contrast, the foam stabilized by nonanionic surfactant

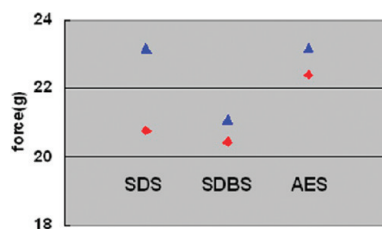


Figure 7. TA results of foam films stabilized by different types of surfactants: ◆, peak compressing force; ▲, viscoelastic force in the pulling procedure. Concentrations of surfactants are all 0.1%wt.

AES did not have this pure drainage process at the beginning and experienced a fairly long drainage procedure ($t_{\text{half}} = 220$ min). The quite slow collapsing process might have been caused by the cooperation of EO groups and anionic groups, the former having an evident interaction with H_2O^{42} and helping to hold more water content.

Figure 5 shows the variation of the overall viscosity of the foam column as a function of time. The circling rotator is believed to bring disturbance to the foam. The dynamic stability of the foam is indicated by the last dot at the end of the apparent viscosity line, which reflects the complete collapse of the foam, and hence the apparent viscosity could not be continuously recorded. Figure 5 shows that, as the gravitational drainage proceeds, the apparent viscosity of the foam column slightly rises during the initial minutes and then begins to decrease along with the collapse of the foam. The foam stabilized by SDS maintained a higher overall apparent viscosity under disturbance by rotation for over 50 min, while the overall apparent viscosity of foam formed from SDBS solution was much lower and decreased rapidly at the same stress force and rotator circling speed, which showed that the latter is dynamically unstable. The dynamic stability of AES foam is a little lower than that of SDS, though it is much better than that of SDBS. Note that the order of apparent viscosity of the three foam systems is consistent with the dynamic stability, which demonstrates that the rheological properties of foam film are supposed to have significant influence on its dynamic stability.

3.2. Experimental Evaluation of Rheological Properties of Foam Films. As shown in Figure 6, the higher elastic modulus and the lower viscous modulus of SDBS foam film demonstrated that the foam film presented stronger stiffness, worse deformability, and poorer capability of maintaining viscosity under the rotary shearing compared to that of SDS foam film. AES foam film has an excellent shear-deformation feature, and its viscoelasticity is as good as that of SDS film reflected by the similar phase angles that they have, even though the viscous modulus of AES foam film is the lowest in the three systems.

RH resulted in rheological information via a rotary way on the horizontal plane, while the TA evaluated foam film from the vertical direction, and the results are well consistent with each other. As foam experienced a drainage process along with the TA determination, the peak viscoelastic force in the pulling procedure is slightly higher than that in the falling procedure for the same system. As shown in Figure 7, SDBS foam tends to have a similar peak compressing force compared with that of SDS foam, while the peak viscoelastic force of SDBS foam is much smaller than that of SDS foam, which indicates the microstiffness of the former film is much larger than the latter one. As for AES, the foam film not only has an excellent viscous feature as well as that

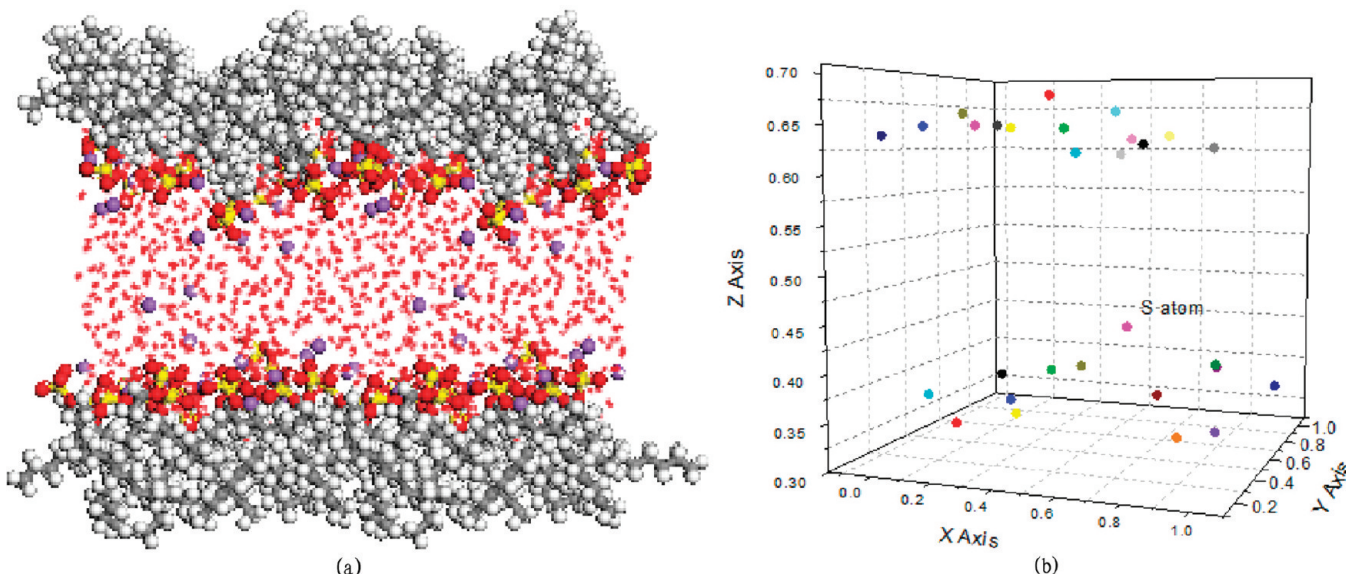


Figure 8. (a) Snapshots of the equilibrium configuration of SDS foam film. The sodium ions are drawn as van der Waals spheres, water molecules are drawn in line style, and the other atoms are drawn in stick style. (b) Three-dimensional distribution of surfactant heads represented by S atoms.

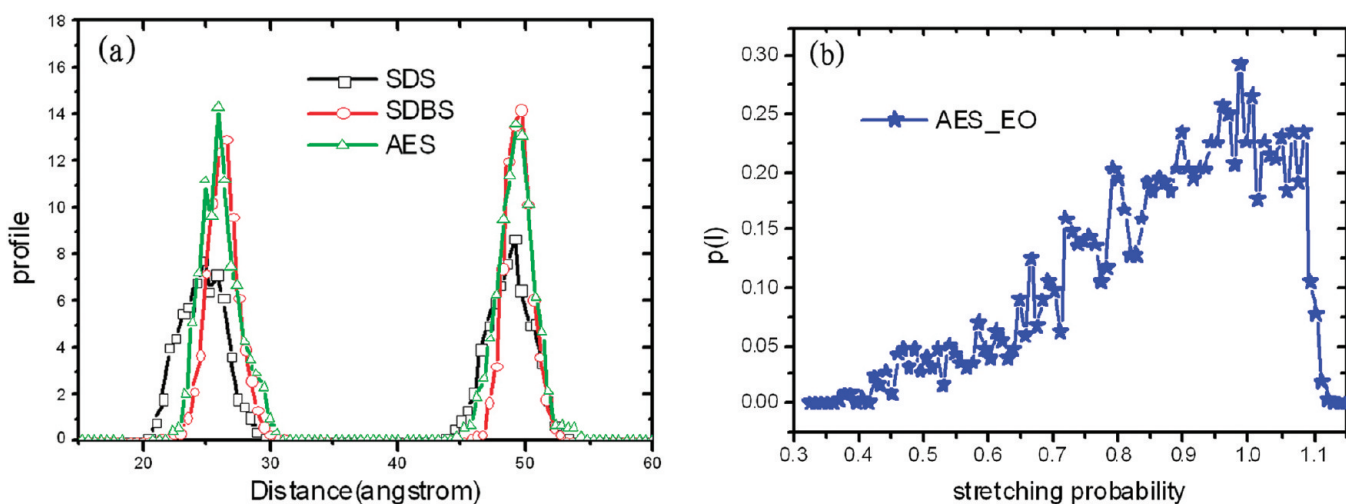


Figure 9. (a) The distribution profiles of surfactant heads along the Z axis at foam films formed by different surfactants. (b) The distribution profile of stretching probability of EO fragments in AES molecules.

of SDS but also shows a higher elasticity than that of SDS foam film. This might be caused by the high thickness of the interface layer and the high water content, which agrees well with the slow drainage phenomenon of AES foam.

Comprehensive analysis of the above results shows that the microstiffness of the foam film should be the key factor which contributes to the static stability of foam while the viscoelasticity of the foam film might play a crucial role on the dynamic stability under disturbance. The molecular simulation results shown below describe the surfactant behavior on the air/water interface and provide a good explanation about the film character of the above foam systems.

3.3. Molecular Simulation Study of Foam Films. *3.3.1. Effect of the Interfacial Distribution of Hydrophilic Heads on Elasticity of Foam Film.* As an example of simulated results, molecular equilibrium geometry of bilayer SDS foam film is shown in Figure 8a. The position of S atoms was used to describe the

distribution of surfactant head groups and the evenness of the foam film (see Figure 8b). The distribution of S atoms along the X and Y axes is wide, and there are many irregular holes occupied by water molecules in the XY plane, while its distribution along the Z axis is relatively narrow. Actually, the areas of the gaps in the XY plane correspond to the number of surfactant molecules packing on the interface, and the distribution along the Z axis determines the varying thickness of the foam film.⁴³

In Figure 9a, the distribution profiles of S atoms along the Z axis in foam films stabilized by SDBS and SDS are different; the former is more regular compared with that of the latter. This can be ascribed to the stronger bond rotation capacity of the linkage O atoms in SDS compared to that of the phenyl group in SDBS, which agree well with the high stiffness of SDBS foam film and the excellent elasticity of SDS foam film. Even though the Z-axis distribution profiles of S atoms in the AES system are similar to that of SDBS, the wide distribution of hydrophilic heads of AES

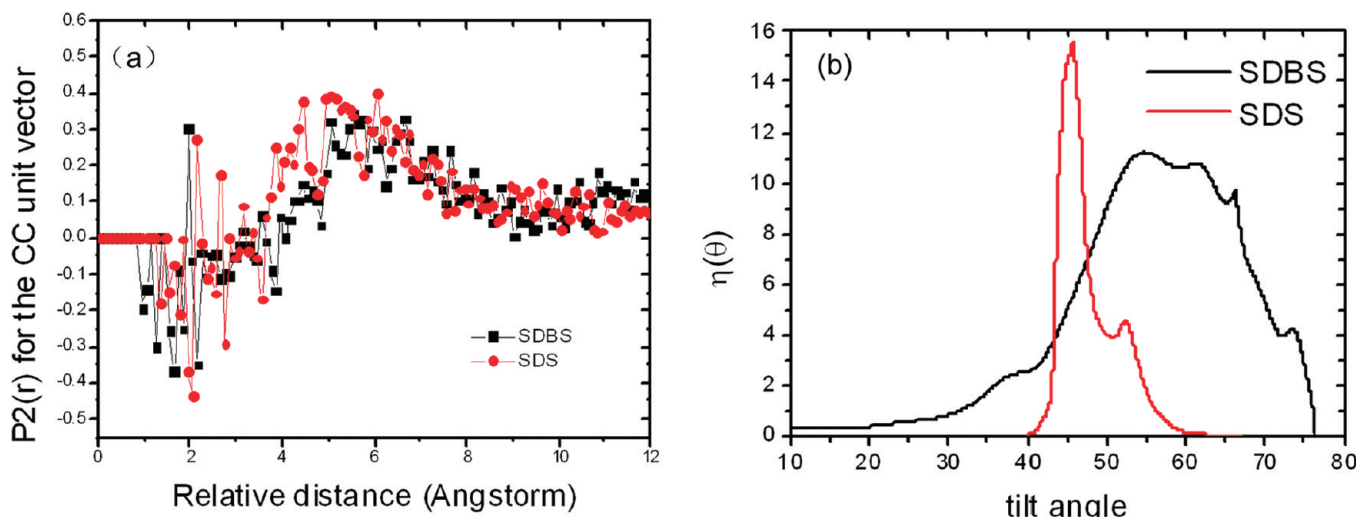


Figure 10. (a) Orientation correlation $P_2(r)$ for the C–C unit vector in different systems. (b) Distribution of the tilt angle θ (in degrees) of the hydrocarbon tails for the two systems with respect to the direction of the normal interface along the z axis.

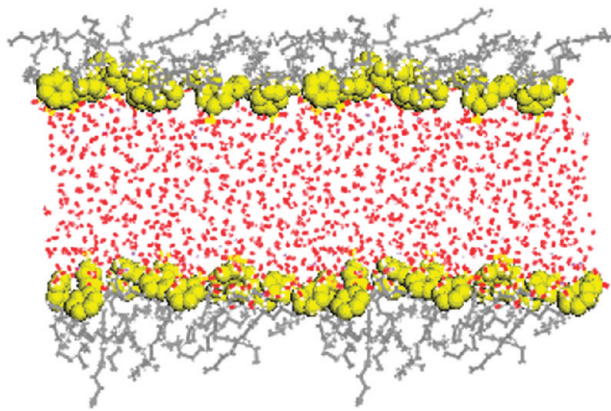


Figure 11. Snapshot of equilibrium configuration of the SDBS foam film. For visual clarity of phenyl, the sodium ions, water molecules, and hydrophobic tails are drawn in line style, while phenyl groups are drawn as CPK.

along the Z axis is inevitable considering that the EO segment distribution is also included. The stretching probability (the ratio of equilibrium length to the initially constructed length; see Figure 9b) of EO segments in AES molecules was distributed in a quite wide range of 0.36–1.12, which indicates that the hydrophilic head chain of AES molecule is fairly elastic; accordingly, the best elasticity of AES foam films is derived from the contribution of the flexible EO segments.

3.3.2. Effect of Interfacial Behavior of Hydrocarbon Tails of Surfactants on the Viscosity and the Microstiffness of Foam Film. To characterize the orientation of the surfactants at the interface, hydrocarbon tail vectors (from the first methylene group CH_2 point to the terminal methyl group CH_3 , abbreviated to be C–C unit vector) were defined, and the orientation correlation⁴⁴ $P_2(r) = \langle \cos^2 \phi_{\vec{\beta}}(r) \rangle - \frac{1}{2}$, which illustrates the parallelism level between the hydrophobic chain (see Figure 10a), was calculated. Furthermore, the distribution of the tilt angle $\eta(\theta)$ ^{45–47} between the vector and the normal line to the XY plane (see Figure 10b) was explored to represent the molecular orientation relative to the interface. All the data are averaged over both monolayers on two sides. On one hand, the orientation

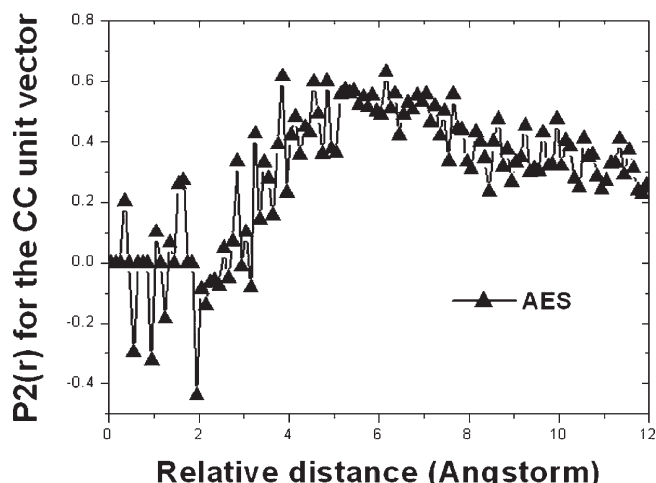


Figure 12. Orientation correlation $P_2(r)$ for the C–C unit vector in the AES foam system.

correlation for the two systems has a slight difference that suggests the crossing degree of the hydrophobic tails is similar. On the other hand, the SDBS tails are more tilted toward the plane of the interface compared to that of SDS, because $\eta(\theta)$ of the former system represents a quite wide range (20° to 75°) compared with that of the latter system (40° to 60°). Moreover, the average tilt angles of SDS and SDBS systems are found to be 45.8° and 59.8° , respectively. This average value of the tilt of the SDS tail is comparable to the experimental value of 45° .^{48,49} Tilt angles of tails of most of the SDBS molecules are in the range $50 \leq \theta \leq 80^\circ$. They represent a flat state with respect to the interface plane, and the anisotropic interface layer is narrower than that of the SDS system.

It is very interesting to note that simulation results show that the tilt angle of the phenyl group of SDBS is about 65° . It can be clearly seen from Figure 11 that all the phenyl groups orient in a similar angle with respect to the interface section along the z axis, occupying the whole exterior of the interface layer. It is the high rigidity of this group that makes the anisotropic interface layer narrower and results in the higher microhardness and lower

viscoelasticity of the SDBS foam film compared to that of SDS molecules. Eventually, the SDBS foam tends to have dynamic stability under disturbance worse than that of the SDS foam.

According to Figure 12, the order of hydrophobic tails of AES in foam film is higher than that of SDS and SDBS induced by the impact of the network forming by EO chains.⁵⁰ Meanwhile, considerable water molecules involved in this network by the hydrogen bond interaction with the flexible EO groups lead to a thick interface layer in AES foam film, which explains the high microelasticity. However, under rotary shearing, the network formed by EO groups and water molecules might be broken, which would bring a decrease of elasticity even faster than that for SDBS. Therefore, the excellent viscoelasticity of AES foam film is contributed mostly by the particularly good microviscosity, which should be an important factor to increase the dynamic stability.

4. CONCLUSION

The relationship of the surfactant molecular structure, behavior, and monolayer configuration in foam film to the apparent foam properties has been elucidated by combining the detailed full-atom simulation method and effective experimental approaches. The surfactants studied in this paper (SDS, SDBS, and AES) can be thought to have similar structures except for the linking groups between the hydrocarbon tails and the sulfonate group. As the O atom is the linking group of SDS, its foam possesses excellent static and dynamic stability. For SDBS, the phenyl rings orient arrisways and occupy all air/water surfaces, leading to higher rigidity and worse deformation of its foam film compared to that of the SDS foam film; therefore, the SDBS foam exhibits poorer dynamic stability and lower apparent viscosity than that of the SDS foam, though the microstiffness of the SDBS foam film leads to its fine static foam stability almost like that of the SDS foam film. From the contribution of flexible EO segments and their special interaction with water molecules, foam film stabilized by the nonanionic surfactant AES presents brilliant elasticity and good microstiffness leading to fine dynamic and static stability, respectively. The microstiffness of foam film contributes to good static stability, while the viscoelasticity of the foam film determines the increase of dynamic stability. The above results help to clarify the foam stabilization mechanism and provide new insights into the contribution to foam properties by surfactant structure.

■ AUTHOR INFORMATION

Corresponding Author

*Tel: +86-531-88362078. Fax: +86-531-88364464. E-mail: yingli@sdu.edu.cn.

■ ACKNOWLEDGMENT

The funding from National Municipal Science and Technology Project (No.2008ZX05011-002) and National Science Fund of China (No. 21173134 and 60876056) is gratefully acknowledged. We express our sincere thanks to Sally Sha, P & G Technologies (Beijing) Ltd., for providing access to the texture analyzer and interfacial shear rheometer.

■ REFERENCES

- (1) Paulson, O.; Pugh, R. J. *Langmuir* **1996**, *12* (20), 4808–4813.
- (2) Binks, B. P. *Curr. Opin. Colloid Interface Sci.* **2002**, *7*, 21–41.
- (3) Farajzadeh, R.; Andrianov, A.; Zitha, P. L. J. *Ind. Eng. Chem. Res.* **2010**, *49* (4), 1910–1919.
- (4) Khrustov, K.; Jachimska, B.; Małysa, K.; Exerowa, D. *Colloids Surf, A* **2001**, *186*, 93–101.
- (5) Stubenrauch, C.; Khrustov, K. J. *Colloid Interface Sci.* **2005**, *286*, 710–718.
- (6) Ruiz-Henestrosa, V. P.; Sánchez, C. C.; Rodríguez Patino, J. M. *J. Agric. Food Chem.* **2008**, *56* (7), 2512–2521.
- (7) Vilkova, N. G.; Kruglyakov, P. M. *Colloids Surf, A* **2005**, *263* (1–3), 205–209.
- (8) Sedev, R.; Exerowa, D. *Adv. Colloid Interface Sci.* **1999**, *83* (1), 111–136.
- (9) Exerowa, D.; Churaev, N. V.; Kolarov, T.; Esipova, N. E.; Panchev, N.; Zorin, Z. M. *Adv. Colloid Interface Sci.* **2003**, *104*, 1–24.
- (10) Trokhymchuk, A.; Henderson, D.; Nikolov, A.; Wasan, D. T. *Langmuir* **2001**, *17* (16), 4940–4947.
- (11) Rippner, B.; Boschkova, K.; Claesson, P. M.; Arnebrant, T. *Langmuir* **2002**, *18* (13), 5213–5221.
- (12) Gibbs, J. W. *Collected Works*; Longmans Green: New York, 1931; Vol. 1.
- (13) Tan, S. N.; Fornasiero, D.; Sedev, R.; Ralston, J. *J. Colloid Interface Sci.* **2005**, *286* (2), 719–729.
- (14) Kovalchuk, V. I.; Miller, R.; Fainerman, V. B.; Loglio, G. *Adv. Colloid Interface Sci.* **2005**, *114*–115, 303–12.
- (15) Monteux, C.; Fuller, G. G.; Bergeron, V. *J. Phys. Chem. B* **2004**, *108*, 16473–16482.
- (16) Espinosa, G.; Langevin, D. *Langmuir* **2009**, *25* (20), 12201–12207.
- (17) Rodríguez-Pérez, M. A.; Campo-Arnáiza, R. A.; Arocab, R. F.; de Saja, J. A. *Polymer* **2005**, *46* (26), 12093–12102.
- (18) Stubenrauch, C.; Albouy, P. A.; Klitzing, R. V.; Langevin, D. *Langmuir* **2000**, *16*, 3206–3213.
- (19) Zumpano, G.; Meo, M. *Comput. Struct.* **2008**, *86* (3–5), 483–490.
- (20) Jang, S. S.; Goddard, W. A., III. *J. Phys. Chem. B* **2006**, *110* (15), 7992–8001.
- (21) Saccani, J.; Castano, S.; Beaurein, F.; Laguerre, M.; Desbat, B. *Langmuir* **2004**, *20* (21), 9190–9197.
- (22) Jang, S. S.; Jang, Y. H.; Kim, Y. H.; Goddard, W. A., III; Choi, J. W.; Heath, J. R.; Laursen, B. W.; Flood, A. H.; Stoddart, J. F.; Nørgaard, K.; Bjørnholm, T. *J. Am. Chem. Soc.* **2005**, *127*, 14804–14816.
- (23) Yang, W. H.; Wu, R. L.; Kong, B.; Zhang, X. F.; Yang, X. Z. *J. Phys. Chem. B* **2009**, *113* (24), 8332–8338.
- (24) Schelero, N.; Hedicke, G.; Linse, P.; Klitzing, R. v. *J. Phys. Chem. B* **2010**, *114* (47), 15523–15529.
- (25) Golemanov, K.; Denkov, N. D.; Tcholakova, S.; Vethamuthu, M.; Lips, A. *Langmuir* **2008**, *24* (18), 9956–9961.
- (26) Lesage, P.; Destain, M. F. *Postharvest Biol. Technol.* **1996**, *8* (1), 45–55.
- (27) Singh, H.; Rockall, A.; Martin, C. R.; Chung, O. K.; Lookhart, G. L. *J. Texture Stud.* **2006**, *37* (4), 383–392.
- (28) Vithanage, C. R.; Grimson, M. J.; Smith, B. G. *J. Texture Stud.* **2009**, *40* (3), 346–369.
- (29) Bischoff White, E. E.; Chellamuthu, M.; Rothstein, J. P. *Rheol. Acta* **2009**, *49* (2), 119–129.
- (30) Li, Y.; Zhang, P.; Zhao, G. Q.; Cao, X. L.; Wang, Q. W.; Wang, H. Y. *Colloids Surf, A* **2006**, *272*, 124–129.
- (31) Du, D. X.; Beni, A. N.; Farajzadeh, R.; Zitha, P. L. J. *Ind. Eng. Chem. Res.* **2008**, *47* (16), 6298–6306.
- (32) Novales, B.; Riaublanc, A.; Navailles, L.; Houssou, B. H.; Gaillard, C.; Nallet, F.; Douliez, J. P. *Langmuir* **2010**, *26* (8), 5329–5334.
- (33) Tarek, M.; Tobias, D. J.; Klein, M. L. *J. Phys. Chem.* **1995**, *99*, 1393.
- (34) Böcker, J.; Schlenkrich, M.; Bopp, P.; Brickmann, J. *J. Phys. Chem.* **1992**, *96*, 9915.
- (35) Bresme, F.; Jordi, F. *Langmuir* **2004**, *20* (12), 5127–5137.
- (36) Rosen, M. J. *Surfactants and Interfacial Phenomena*, 3rd ed.; Wiley-Interscience: New York, 2004.
- (37) Hwang, M. J.; Stockfisch, T. P.; Hagler, A. T. *J. Am. Chem. Soc.* **1994**, *116* (6), 2515–2525.

- (38) Maple, J. R.; Hwang, M. J.; Stockfisch, T. P.; Dinur, U.; Waldman, M.; Ewig, C. S.; Hagler, A. T. *J. Comput. Chem.* **1994**, *15* (2), 162–182.
- (39) Peng, Z.; Ewig, C. S.; Hwang, M. J.; Waldman, M.; Hagler, A. T. *J. Phys. Chem. A* **1997**, *101* (39), 7243–7252.
- (40) Frenkel, D.; Smit, B. *Understanding Molecular Simulations*, 2nd ed.; Academic Press: London, U.K., 2002.
- (41) Heuser, J.; Moller, J.; Spendel, W.; Pace, G. *Langmuir* **2008**, *24* (20), 11414–11421.
- (42) Holmes, M. C. *Curr. Opin. Colloid Interface Sci.* **1998**, *3* (5), 485–492.
- (43) Karakashev, S. I.; Nguyen, P. T.; Tsekov, R.; Hampton, M. A.; Nguyen, A. V. *Langmuir* **2008**, *24* (20), 11587–11591.
- (44) Baaden, M.; Burgard, M.; Wipff, G. *J. Phys. Chem. B* **2001**, *105* (45), 11131–11141.
- (45) Cox, S. J.; Alonso, M. D.; Weaire, D. *Eur. Phys. J. E* **2006**, *19* (1), 17–22.
- (46) Mishra, N. C.; Müllera, H. J.; Möhwald, H.; Krastev, R. *Colloids Surf, A* **2006**, *282*–*283*, 92–98.
- (47) Koehler, S. A.; Hilgenfeldt, S.; Weeks, E. R.; Stone, H. A. *Phys. Rev. E* **2002**, *66* (4), 040601(R).
- (48) Lu, J. R.; Su, T. J.; Li, Z. X.; Thomas, R. K.; Staples, E. J.; Tucker, I.; Penfold, J. *J. Phys. Chem. B* **1997**, *101* (49), 10332–10339.
- (49) Shi, L.; Tummala, N. R.; Striolo, A. *Langmuir* **2010**, *26* (8), 5462–5474.
- (50) Holmes, M. C. *Curr. Opin. Colloid Interface Sci.* **1998**, *3* (5), 485–492.